Loudspeaker Virtualization–Part I: Digital Modeling and Implementation of the Nonlinear Transducer Equivalent Circuit

Alberto Bernardini[a,*], Lucio Bianchi[b], Augusto Sarti[a]

[a] *Dipartimento di Elettronica, Informazione e Bioingegneria (DEIB), Politecnico di Milano, Piazza L. Da Vinci 32, 20133 Milano, Italy*
[b] *Elettromedia s.p.a., Strada Regina km 3.500, 62018 Potenza Picena (MC), Italy*

Abstract

This manuscript, the first of a two-part series, presents a methodology for efficiently implementing an equivalent circuit of nonlinear loudspeakers in the discrete-time domain. This is a crucial step that will allow us to design new algorithms for loudspeaker virtualization in part II of this series. The presented implementation, in fact, is based on Wave Digital Filter (WDF) principles, which lead to a *fully explicit* model, in the sense that no iterative solvers are needed to compute the output signal. The proposed WDF is highly efficient and modular, since the reference circuit is modeled as a computable interconnection of input-output processing blocks. The accuracy of the implementation is confirmed by comparing it to a ground-truth SPICE simulation of the reference circuit and to measurements on real loudspeakers. This confirms that the proposed Wave Digital modeling approach can be reliably used for the rapid simulation of the transduction behavior of a loudspeaker (within the frequency limits of validity of the equivalent circuit), and can be employed to develop the digital preprocessing method for loudspeaker virtualization described in the second manuscript of this two-part series.

Keywords: Nonlinear Loudspeaker Modeling, Wave Digital Filters

*Corresponding author
Email addresses: alberto.bernardini@polimi.it (Alberto Bernardini), lucio.bianchi@elettromedia.it (Lucio Bianchi), augusto.sarti@polimi.it (Augusto Sarti)

2010 MSC: 00-01, 99-00

1. Introduction

Loudspeakers are electroacoustic transducers whose dynamics is characterized by coupled multiphysical phenomena (mechanical, magnetic, electrical, thermodynamic, and acoustic) [1]. Nonidealities in the loudspeaker transduction process often cause nonlinear distortion, affecting the quality of sound, especially in the low-frequency range, when high-magnitude audio signals are involved [2]. Building models of loudspeakers that are simultaneously accurate and efficient is a challenging task. Such models are useful both for transducer design purposes, and for the development of loudspeaker equalization, linearization or virtualization algorithms based on digital signal processing [3, 4, 5, 6, 7, 8, 9, 10, 11, 12, 13]. Particularly with the latter class of algorithms, the simulation processing is expected to be so efficient as to be suitable for on-the-fly operation.

Several kinds of loudspeaker models are available in the literature. Some rely on *black-box* system identification procedures, such as neural networks [14], NARMAX models [15], Volterra models [3, 16] or Volterra-Wiener-Hammerstein models [17]. These models are generally very flexible and efficient to run, however they lack a physical interpretation and the estimation of their parameters from input/output data is often a cumbersome process, especially dealing with high-order filters.

Another class of modeling methods is based on *white-box* approaches that provide a physical representation of the transduction phenomenon using differential equations. In particular, lumped electrical equivalent circuits can be employed to accurately describe the nonlinear low-frequency behavior of loudspeakers by using a set of physically interpretable parameters [18, 19, 20, 21, 22, 2, 23, 24, 25]. The circuital models of loudspeakers that are most frequently employed, both in academia and in industry, are based on the pioneering works by Thiele and Small [18, 26, 19, 20]. These early works discuss linear modeling

approaches that are accurate just when considering low-amplitude signals. Such circuital models have been later extended in various ways in order to describe the behavior of loudspeakers driven by high-amplitude signals, specifically by including different nonlinearities characterized by polynomial functions of the voice coil displacement [2]. In some publications [22, 27], the low-frequency circuital description of the transducer is made of two interdependent subcircuits. This is often the case when the loudspeaker is installed in an infinite baffle configuration [23, Chapter 15], [24, Chapter 6]. The first subcircuit represents the electrical part of the transducer and it is coupled with the second subcircuit representing the mechanical part through a transformer or gyrator. Considering loudspeakers with enclosure, e.g., a closed box, in addition to the two aforementioned subcircuits, the low-frequency electrical equivalent often also includes a third subcircuit that is coupled with the mechanical one and is characterized by acoustical parameters depending on the geometric properties of the enclosure [23, Chapter 16], [24, Chapter 7]. Nonlinear extensions of the Thiele-Small model presented in [2] are still considered the most effective compromise between accuracy and efficiency and have been employed in many recent publications on the digital modeling of acoustic transducers [28, 29, 30, 31, 32, 33, 27, 14].

Once a suitable electrical equivalent of the loudspeaker has been chosen, its parameters are estimated by employing well established system identification methods [34] and, eventually, measuring the acoustical parameters related to the geometry of the transducer cabinet. Small-signal analysis is performed to estimate the linear Thiele-Small parameters, e.g., by employing the measurement of the electric input impedance [26, 19, 18]. The estimation of nonlinear parameters, instead, is done by using large-signal analysis methods and solving nonlinear optimization problems [35, 34]. One of the most widespread tools to estimate the parameters of a nonlinear electrical equivalent of transducers based on the sensing of physical quantities is the Klippel Analyzer System [34], which measures the linear and nonlinear parameters of the lumped model by sensing the electric input current, the electric input voltage, and the voice coil displacement, and finally solving a nonlinear optimization problem using the approach

described in [35].

In the Kirchhoff domain, i.e., the domain of voltage and current variables, when stable implicit discretization methods, like the trapezoidal rule or the Backward Euler method, are used to approximate time derivatives and time integrals, discrete-time representations of nonlinear equivalent circuits of loudspeakers are characterized by systems of implicit equations [25]. It follows that their implementation requires the use of nonlinear iterative solvers, which are not always suitable to be employed in digital signal processing algorithms with strong constraints on efficiency and robustness, because their convergence is not guaranteed and the number of needed iterations per sample is difficult to estimate a-priori.

An alternative approach to the discrete-time implementation of equivalent circuits is based on Wave Digital Filter (WDF) principles [36]. The literature on WDFs has shown that modeling a circuit in the Wave Digital (WD) domain might bring advantages over Kirchhoff domain approaches in terms of efficiency, good numerical properties, and robustness of the digital realization of the reference system [36, 37, 38, 39, 40, 41]. Among the many perks of WDF modeling is the possibility to turn discrete-time models of circuits, which are implicit in the Kirchhoff domain, into explicit WDF models based on the same stable discretization methods [42]. In the literature on electroacoustic transducer modeling, WDF principles have been already used in [22] to derive an explicit discrete-time realization of a model composed of two coupled subcircuits describing the electrical and the mechanical parts of the loudspeaker.

In this manuscript, we consider the circuital model of loudspeakers in Fig. 1 composed of three subcircuits; one for the electrical part, one for the mechanical part, and one representing the acoustical behavior of the enclosure. The lumped model contains three nonlinearities, all characterized by polynomial functions of the diaphragm displacement as discussed in [2]: the force factor, the inductive part of the voice coil impedance, and the mechanical stiffness. It is worth recalling that the considered lumped description of the transduction process is accurate when dealing with low-frequency audio signals [18, 24]. In fact,

according to [24, pp. 279-280], the lumped model considers the diaphragm as a planar piston that moves with uniform velocity over the entire surface. This approximation is valid if the depth of the diaphragm is less than about one-tenth of the wavelength of the sound waves of interest. Under the assumption of dealing with low-frequency audio signals, the model in Fig. 1 is quite general, and is capable of describing loudspeakers of different sizes and kinds of enclosures [26, 19, 18, 23, 24, 27, 29, 30, 31]. The considered nonlinear model is then realized using a novel fully explicit WDF which does not require any iterative solver to be implemented. The WDF discussed in this manuscript is an essential building block of the loudspeaker virtualization algorithm extensively described in the second part [43] of this two-part work. The present manuscript is therefore self-contained, even though important applications of the presented WDF model of loudspeakers are discussed in the companion article [43].

The structure of the manuscript is the following. Section 2 describes the linear version of the employed equivalent circuit model of transducers and Section 3 discusses an explicit WDF realization of it. Section 4 describes a nonlinear extension of the model in Section 2 and Section 5 presents its corresponding explicit WDF implementation. Section 6 concludes this manuscript.

2. Linear Loudspeaker Model

In this section we consider a linear version of the circuit equivalent model of loudspeakers shown in Fig. 1, while in Section 4 we will describe a possible extension where nonlinearities and further interdependencies between circuit variables will be introduced. The considered linear model is suitable for describing the behavior of transducers when excited with low-amplitude signals [2].

The circuit is made of three subcircuits (referring to the electrical part, the mechanical part, and the acoustical part of the system, respectively) [19], each depending on the others. The circuital equivalent is derived according to the impedance analogy, where mechanical velocity and acoustical volume velocity

are represented by electrical currents; and mechanical force and acoustical pressure are represented by electrical voltages.

The first subcircuit representing the electrical part is composed of the following elements in series: a voltage generator with signal V_{in} that is the input voltage applied to the loudspeaker; a resistor with resistance R_{e} that represents the resistive part of the voice coil impedance; an inductor with inductance L_{e} that models the inductive part of the voice coil impedance; a current-controlled voltage source that is controlled by the diaphragm velocity signal I_{ms} weighted by the so called *force factor* Bl.

The second subcircuit representing the mechanical part is composed of the following elements in series: an inductor with inductance M_{ms} that models the mass of all the moving components; a resistor with resistance R_{ms} that refers to the mechanical resistance; a capacitor with capacitance $C_{\mathrm{ms}} = K_{\mathrm{ms}}^{-1}$ that refers to the mechanical compliance, where K_{ms} is the mechanical stiffness; a current-controlled voltage source that is controlled by the current signal I_{e} weighted by the force factor Bl; a voltage-controlled voltage source that is controlled by the pressure signal P_{out} weighted by the parameter S_{d} indicating the effective piston area which represents the diaphragm radiating surface.

The third subcircuit representing the acoustical part is composed of: a capacitor with capacitance C_{cab} that models the acoustic compliance of the cabinet; a resistor with resistance R_{cab} that models the acoustic resistance of the cabinet; a resistor with resistance R_{al} that represents a further acoustic damping; a current-controlled current source controlled by the diaphragm velocity I_{ms} weighed by the parameter S_{d}.

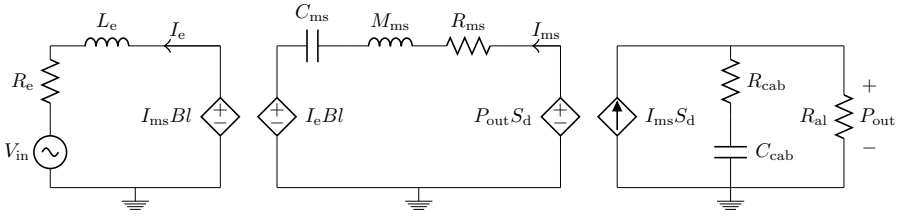

Figure 1: Transducer equivalent circuit.

Table 1: Linear Model: Constitutive Equations of One-Port Circuit Elements

Element	**Constitutive Equation**	**Element**	**Constitutive Equation**
V_{in}, R_{e}	$v(t) = V_{\mathrm{in}}(t) + R_{\mathrm{e}} i(t)$	R_{ms}	$v(t) = R_{\mathrm{ms}} i(t)$
L_{e}	$v(t) = L_{\mathrm{e}} \frac{\mathrm{d}i(t)}{\mathrm{d}t}$	R_{cab}	$v(t) = R_{\mathrm{cab}} i(t)$
K_{ms}	$i(t) = \frac{1}{K_{\mathrm{ms}}} \frac{\mathrm{d}v(t)}{\mathrm{d}t}$	C_{cab}	$i(t) = C_{\mathrm{cab}} \frac{\mathrm{d}v(t)}{\mathrm{d}t}$
M_{ms}	$v(t) = M_{\mathrm{ms}} \frac{\mathrm{d}i(t)}{\mathrm{d}t}$	R_{al}	$v(t) = R_{\mathrm{al}} i(t)$

As the WDF implementation discussed in the next Section is based on a port-wise consideration of the circuit, we collect in Table 1 the local constitutive equations of the one-port circuit elements. Each one-port circuit element is characterized by a continuous-time constitutive equation relating its port voltage $v(t)$ to its port current $i(t)$, where t is the time variable in seconds. In this section all the circuit elements are assumed to be linear. The voltage generator V_{in} is combined with the resistance R_{e} and the two are treated as a one-port resistive voltage source. The resistive voltage source, L_{e}, K_{ms}, M_{ms}, R_{ms}, R_{cab}, C_{cab}, R_{al} are modeled as one-port elements.

As far as the controlled sources are concerned, they form two two-ports. The first two-port is an ideal gyrator with gyration factor Bl. It is composed of the current-controlled voltage source that delivers the signal $I_{\mathrm{ms}}Bl$ in the subcircuit representing the electrical part and the current-controlled voltage source that delivers the signal $I_{\mathrm{e}}Bl$ in the subcircuit representing the mechanical part. The second two-port is an ideal transformer with turn ratio S_{d}. It is composed of the voltage-controlled voltage source that delivers the signal $P_{\mathrm{out}}S_{\mathrm{d}}$ in the subcircuit representing the mechanical part and the current-controlled current source that delivers the signal $I_{\mathrm{ms}}S_{\mathrm{d}}$ in the subcircuit representing the mechanical part.

As an example, Table 2 reports the values of the electrical equivalent parameters of two loudspeaker systems with drivers of significantly different sizes. The first (named "Spk-1" in the rest of the manuscript) is characterized by a LaVoce FSF122.02-8, which is a 12 inch fullrange driver with ferrite magnet,

Table 2: Parameters of Linear Circuital Model and Corresponding Values

Param.	**Spk-1**	**Spk-2**	**Param.**	**Spk-1**	**Spk-2**
R_{e} [Ω]	5.91	3.29	R_{cab} $\left[\frac{\mathrm{kg}}{\mathrm{m}^4\mathrm{s}}\right]$	18.7072	136.9273
L_{e} [mH]	0.547	0.036	C_{cab} $\left[\frac{\mathrm{m}^4\mathrm{s}^2}{\mathrm{kg}}\right]$	0.0000071487	0.0000071487
K_{ms} $\left[\frac{\mathrm{N}}{\mathrm{mm}}\right]$	4.99	1.54	R_{al} $\left[\frac{\mathrm{kg}}{\mathrm{m}^4\mathrm{s}}\right]$	3741.4	1369.3
M_{ms} [g]	38.606	1.476	Bl $\left[\frac{\mathrm{N}}{\mathrm{A}}\right]$	13.854	2.219
R_{ms} $\left[\frac{\mathrm{kg}}{\mathrm{mm}}\right]$	2.814	0.344	S_{d} [cm^2]	539.13	17.87

steel basket, and 300 W program power handling. The second (named "Spk-2" in the rest of the manuscript) is characterized by a LaVoce FSN020.71-4, which is a 2 inch fullrange driver with neodymium magnet, steel basket, and 30 W program power handling. The circuital model parameters of both loudspeakers are measured using the Klippel Analyzer System [34, 44].

3. Wave Digital Realization of the Linear Loudspeaker Model

In this section we discuss the WD realization of the reference circuit in Fig. 1. We start by presenting the scattering relations of WD linear one-ports, we then model the WD junctions, and we finally describe the signal flow used for the implementation of the resulting WD structure shown in Fig. 2.

Circuit elements are represented with one-port input-output blocks, while WD junctions $\mathcal{R}_1$, $\mathcal{P}_1$, $\mathcal{S}_1$, $\mathcal{S}_2$, and $\mathcal{S}_3$ are represented with multi-port input-output blocks. Ports of WD junctions are named with the numbers in gray in Fig. 2; the numbers are chosen without any precise ordering criterion. It is worth noting that, in order to not overcomplicate the WD model representation and, consequently, the notation, we decided not to put numbers on ports of circuit elements. The sampling frequency of the WDF simulations is defined as $F_{\mathrm{s}} = 1/T_{\mathrm{s}}$, where T_{s} is the sampling period.

3.1. WD Modeling of Circuit Elements

Assuming that time derivatives are approximated with stable linear multi-step discretization methods (e.g., trapezoidal rule, backward Euler or higher

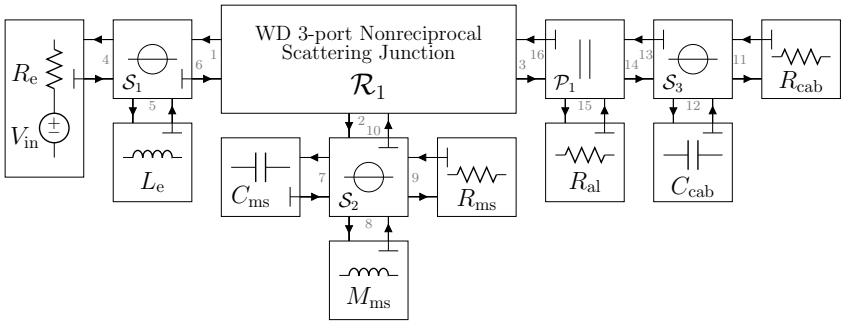

Figure 2: WDF realization of the transducer circuital model.

order backward differentiation formulas), each Kirchhoff constitutive equation in the continuous-time domain in Table 1 can be expressed in the discrete-time domain using the following formula [42] referred to a general time-varying voltage generator

$$v[k] = R_\mathrm{g}[k]i[k] + V_\mathrm{g}[k] \ , \tag{1}$$

where the variable $k \in \mathbb{Z}$ in square brackets indicates the discrete-time sample index, $v[k]$ is the port voltage, $i[k]$ is the port current, $V_\mathrm{g}[k]$ is the source and $R_\mathrm{g}[k]$ is the series resistance. Let us then apply the following transformation of port variables [36]

$$v[k] = \frac{a[k] + b[k]}{2} \ , \quad i[k] = \frac{a[k] - b[k]}{2Z[k]} \ , \tag{2}$$

where $a[k]$ is the wave incident to the element, $b[k]$ is the wave reflected from the element and $Z[k] > 0$ is a free parameter called reference port resistance. Substituting (2) in (1) and then expressing $b[k]$ as a function of $a[k]$ we get [42]

$$b[k] = \left(\frac{R_\mathrm{g}[k] - Z[k]}{R_\mathrm{g}[k] + Z[k]}\right) a[k] + \left(\frac{2Z[k]}{R_\mathrm{g}[k] + Z[k]}\right) V_\mathrm{g}[k] \ . \tag{3}$$

We notice that if we set $Z[k] = R_\mathrm{g}[k]$ the instantaneous dependence of $b[k]$ from $a[k]$ is eliminated; in this case, the element is said to be *adapted* and the scattering relation (3) reduces to

$$b[k] = V_\mathrm{g}[k] \qquad \text{with} \qquad Z[k] = R_\mathrm{g}[k]. \tag{4}$$

Table 3: Implementation of WD One-Ports

	Imposed Constraint	**Scattering Relation**
V_{in}, R_{e}	$Z = R_{\text{e}}$	$b[k] = V_{\text{in}}[k]$
L_{e}	$Z = L_{\text{e}} F_s$	$b[k] = (b[k-1] - a[k-1])/2$
K_{ms}	$Z = K_{\text{ms}} T_{\text{s}}$	$b[k] = (b[k-1] + a[k-1])/2$
M_{ms}	$Z = M_{\text{ms}} F_s$	$b[k] = (b[k-1] - a[k-1])/2$
R_{ms}	$Z = R_{\text{ms}}$	$b[k] = 0$
R_{cab}	$Z = R_{\text{cab}}$	$b[k] = 0$
C_{cab}	$Z = T_{\text{s}}/C_{\text{cab}}$	$b[k] = (b[k-1] + a[k-1])/2$
R_{al}	$Z = R_{\text{al}}$	$b[k] = 0$

Table 3 shows the scattering relations of all the WD one-port elements of the linear loudspeaker model that are all particular cases of (4). Time derivatives of dynamic elements (inductors and capacitors) are discretized using the backward Euler method according to the formulas presented in [42].

3.2. WD Modeling of Connection Networks

In the WD domain, a N-port connection network is modeled as a N-port junction characterized by a $N \times N$ scattering matrix $\mathbf{S}$ such that $\mathbf{b} = \mathbf{S}\mathbf{a}$, where $\mathbf{a} = \mathbf{v} + \mathbf{Z}\mathbf{i}$ is the vector of waves incident to the junction, $\mathbf{b} = \mathbf{v} - \mathbf{Z}\mathbf{i}$ is the vector of waves reflected from the junction, $\mathbf{v}$ is the vector of port voltages, $\mathbf{i}$ is the vector of port currents and $\mathbf{Z}$ is a diagonal matrix containing the free parameters [45, 40, 46, 47].

Series and parallel connections are implemented using series and parallel adaptors well established in WDF theory [36, 46].

As an example, let us consider the 3-port series adaptor $\mathcal{S}_1$ whose port numbers are 4, 5, and 6; hence the vector of waves incident to the junction, the vector of waves reflected from the junction, and the diagonal matrix of port resistances are $\mathbf{a}_{\mathcal{S}_1} = [a_4, a_5, a_6]^T$, $\mathbf{b}_{\mathcal{S}_1} = [b_4, b_5, b_6]^T$, and $\mathbf{Z}_{\mathcal{S}_1} = \text{diag}[Z_4, Z_5, Z_6]$, respectively. Port 6 is made reflection-free, i.e., the third diagonal entry of the scattering matrix is set to zero, by imposing $Z_6 = Z_4 + Z_5$. The scattering

matrix of $\mathcal{S}_1$ is expressed as [36]

$$\mathbf{S}_{\mathcal{S}_1} = \begin{bmatrix} \frac{Z_5}{Z_4+Z_5} & \frac{-Z_4}{Z_4+Z_5} & \frac{-Z_4}{Z_4+Z_5} \\ \frac{-Z_5}{Z_4+Z_5} & \frac{Z_4}{Z_4+Z_5} & \frac{-Z_5}{Z_4+Z_5} \\ -1 & -1 & 0 \end{bmatrix} . \tag{5}$$

We can similarly derive also the scattering matrix of the 3-port series adaptor $\mathcal{S}_3$, whose port numbers are 11, 12, and 13. Port 13 is made reflection-free by setting $Z_{13} = Z_{11} + Z_{12}$.

The ports of the 4-port series adaptor $\mathcal{S}_2$ are named 7, 8, 9, and 10; hence we have $\mathbf{a}_{\mathcal{S}_2} = [a_7, a_8, a_9, a_{10}]^T$, $\mathbf{b}_{\mathcal{S}_2} = [b_7, b_8, b_9, b_{10}]^T$, and $\mathbf{Z}_{\mathcal{S}_2} = \mathrm{diag}[Z_7, Z_8, Z_9, Z_{10}]$. Port 10 is made reflection-free by imposing $Z_{10} = Z_7 + Z_8 + Z_9$. The scattering matrix of $\mathcal{S}_2$ is expressed as [46]

$$\mathbf{S}_{\mathcal{S}_2} = \begin{bmatrix} \frac{Z_8+Z_9}{Z_7+Z_8+Z_9} & \frac{-Z_7}{Z_7+Z_8+Z_9} & \frac{-Z_7}{Z_7+Z_8+Z_9} & \frac{-Z_7}{Z_7+Z_8+Z_9} \\ \frac{-Z_8}{Z_7+Z_8+Z_9} & \frac{Z_7+Z_9}{Z_7+Z_8+Z_9} & \frac{-Z_8}{Z_7+Z_8+Z_9} & \frac{-Z_8}{Z_7+Z_8+Z_9} \\ \frac{-Z_9}{Z_7+Z_8+Z_9} & \frac{-Z_9}{Z_7+Z_8+Z_9} & \frac{Z_7+Z_8}{Z_7+Z_8+Z_9} & \frac{-Z_9}{Z_7+Z_8+Z_9} \\ -1 & -1 & -1 & 0 \end{bmatrix} . \tag{6}$$

The three ports of the parallel adaptor $\mathcal{P}_1$ are 14, 15, and 16; hence we have $\mathbf{a}_{\mathcal{P}_1} = [a_{14}, a_{15}, a_{16}]^T$, $\mathbf{b}_{\mathcal{P}_1} = [b_{14}, b_{15}, b_{16}]^T$, and $\mathbf{Z}_{\mathcal{P}_1} = \mathrm{diag}[Z_{14}, Z_{15}, Z_{16}]$. Port 16 of $\mathcal{P}_1$ is made reflection-free by imposing $Z_{16} = (Z_{14}Z_{15})/(Z_{14} + Z_{15})$. The scattering matrix of $\mathcal{P}_1$ is expressed as [36]

$$\mathbf{S}_{\mathcal{P}_1} = \begin{bmatrix} \frac{-Z_{14}}{Z_{14}+Z_{15}} & \frac{Z_{14}}{Z_{14}+Z_{15}} & 1 \\ \frac{Z_{15}}{Z_{14}+Z_{15}} & \frac{-Z_{15}}{Z_{14}+Z_{15}} & 1 \\ \frac{Z_{15}}{Z_{14}+Z_{15}} & \frac{Z_{14}}{Z_{14}+Z_{15}} & 0 \end{bmatrix} . \tag{7}$$

As pointed out in [40], when implementing circuits with multi-port linear elements, it might be convenient in terms of computability to embed such elements inside junctions. We opt for this strategy and we consider a 3-port connection network that absorbs the two controlled sources as shown in Fig. 3. The three ports of the connection network are named 1, 2, and 3. Since the connection network in Fig. 3 is non-reciprocal we follow the approach described in [40] in order to derive the scattering matrix $\mathbf{S}_{\mathcal{R}_1}$ of the WD junction $\mathcal{R}_1$ and we obtain

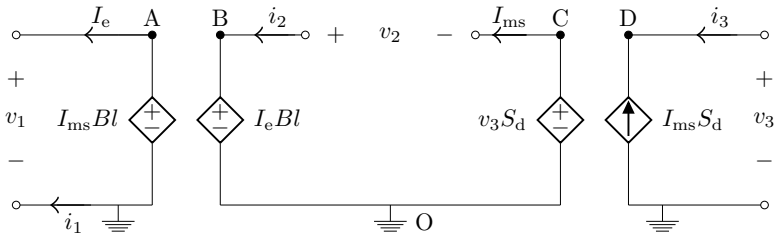

Figure 3: 3-port connection network implemented with WD $\mathcal{R}_1$ adaptor.

$$\mathbf{S}_{\mathcal{R}_1} = \rho \begin{bmatrix} Bl^2 - Z_1Z_3S_\mathrm{d}^2 - Z_1Z_2 & -2BlZ_1 & 2BlS_\mathrm{d}Z_1 \\ 2BlZ_2 & Bl^2 + Z_1Z_3S_\mathrm{d}^2 - Z_1Z_2 & 2S_\mathrm{d}Z_1Z_2 \\ -2BlS_\mathrm{d}Z_3 & 2S_\mathrm{d}Z_1Z_3 & Bl^2 - Z_1Z_3S_\mathrm{d}^2 + Z_1Z_2 \end{bmatrix} \tag{8}$$

where $\rho = (Bl^2 + Z_1Z_3S_\mathrm{d}^2 + Z_1Z_2)^{-1}$.

3.3. Implementation of the WD Structure

In the previous two subsections we discussed how to locally model one-port elements and connection networks as input-output blocks characterized by scattering relations. In this subsection we show how the WD structure in Fig. 2 can be globally implemented in such a way that we can solve the reference circuit at each sampling step without using any iterative solver. Before presenting the signal flow in the structure, we describe how two WD blocks can be linked through a port connection. Let us consider, as an example, the port connection between the two WD junctions $\mathcal{S}_1$ and $\mathcal{R}_1$. If a_6 and b_6 are the incident and reflected waves to $\mathcal{S}_1$, respectively; and if a_1 and b_1 are the incident and reflected waves to $\mathcal{R}_1$, respectively; the port connection between $\mathcal{S}_1$ and $\mathcal{R}_1$ is obtained by setting the following constraints

$$a_1 = b_6 \quad , \quad b_1 = a_6 \quad , \quad Z_1 = Z_6 \ . \tag{9}$$

Similarly, a one-port WD element can be connected to the port of a WD junction by applying the same sort of constraints.

The strategy used for the implementation of the WD structure in Fig. 2 is similar to the one explained in [48] where WDFs are treated as connection trees with a root, nodes, and leaves. In our case, the leaves are all the adapted one-ports, the nodes are the series and the parallel adaptors while the root is $\mathcal{R}_1$. At each sampling step, waves reflected from the leaves are propagated toward the root through the nodes using scattering relations. The three incident waves facing the root are computed, so that that the three reflected waves can be readily computed via matrix-vector multiplication. A backward path is then taken by the wave signals scattered through the nodes from the root toward the leaves, so that the incident waves to all the one-ports can be computed. This process is performed at each sampling step in a completely explicit fashion, i.e., no iterative solvers are used. This is possible because all the instantaneous relations between port variables have been eliminated by properly setting the free parameters in such a way that some ports of the WD blocks are made reflection-free. T-shaped symbols in Fig. 2 indicate reflection-free ports, in accordance to the graphical notation used in traditional WDFs [36].

3.4. Linear WDF Model Validation

In this subsection, we validate the behavior of the linear WDF model; firstly, by comparing the results of its MATLAB implementation to SPICE simulations performed with the Electrical Circuit interface of COMSOL Multiphysics, and then by comparing them to measured signals of the two real loudspeaker systems Spk-1 and Spk-2 driven with low-amplitude signals. In particular, the loudspeaker input voltage V_{in} is a multi-tone composed of multiple sinusoids whose fundamental frequencies are selected in such a way that we have 24 values per octave and amplitude is 0.3 V_{rms}. The employed measurement setup is described in Appendix A. The circuital parameters used in the simulations and referring to the two considered loudspeakers are reported in Table 2. The sampling frequency set in the WDF simulations is $F_{\text{s}} = 96$ kHz.

Fig. 4 shows the validation results in the domain of temporal frequency f. The subfigure on the left refers to Spk-1, while the subfigure on the right to Spk-

2. The upper plots include the amplitude response of the electrical impedance, defined as $|\mathcal{Z}_{\mathrm{e}}(f)|= |\mathcal{V}_{\mathrm{in}}(f)|/|\mathcal{I}_{\mathrm{e}}(f)|$, where $\mathcal{V}_{\mathrm{in}}(f)$ and $\mathcal{I}_{\mathrm{e}}(f)$ are the computed Fourier transforms of $V_{\mathrm{in}}(t)$ and $I_{\mathrm{e}}(t)$, respectively. The lower plots show the amplitude response of the output pressure signal $|\mathcal{P}_{\mathrm{out}}(f)|$, where $\mathcal{P}_{\mathrm{out}}(f)$ is the Fourier transform of $P_{\mathrm{out}}(t)$. Upper and lower plots also include pairs of curves of the absolute error between measured data and SPICE, and between measured data and WDF. Both absolute errors are normalized w.r.t. measured data and expressed in percentage. The vertical green lines represent frequency thresholds below which the used lumped model is assumed to be valid, in accordance to the analysis provided in [24, pp. 279-280] which considers the diaphragm as a planar piston that moves with uniform velocity over the entire surface. The frequency thresholds are estimated using the formula $f_{\mathrm{thr}} = c/(10d)$, where c is the speed of sound and d is the speaker cone depth.

We generally notice that there is a near-perfect correspondence between the results of WDF and SPICE simulations. Also the matching between simulations and measured data is very good, as confirmed by the normalized absolute errors that are almost always under 10%, when frequencies below f_{thr} are considered.

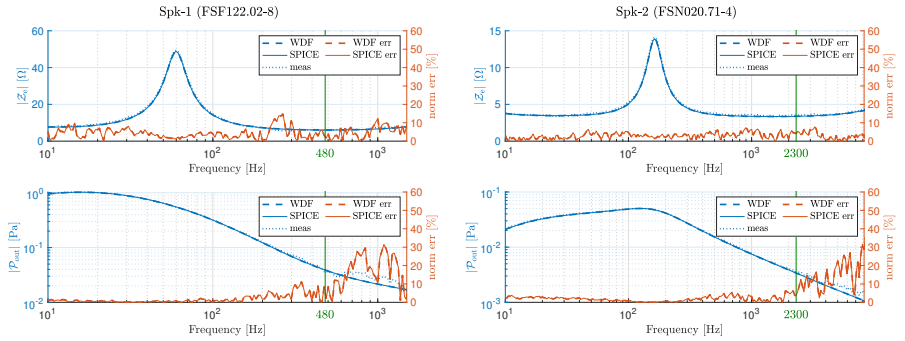

(a) (b)

Figure 4: Linear model validation. Measured and simulated amplitude frequency responses of electric impedance $|\mathcal{Z}_{\mathrm{e}}|$ and output pressure $|\mathcal{P}_{\mathrm{out}}|$ (in blue), along with normalized absolute errors in percentage between measured data and WDF simulation results, and between measured data and SPICE simulation results (in red). (a) refers to Spk-1. (b) refers to Spk-2.

Table 4: Coefficients of Force Factor, Inductor, and Mechanical Stiffness Polynomials

Coef.	**Spk-1**	**Spk-2**	**Coef.**	**Spk-1**	**Spk-2**
Bl_0 $\left[\frac{\mathrm{N}}{\mathrm{A}}\right]$	13.854	2.219	$K_{\mathrm{ms}0}$ $\left[\frac{\mathrm{N}}{\mathrm{mm}}\right]$	4.99	1.54
Bl_1 $\left[\frac{\mathrm{N}}{\mathrm{Amm}}\right]$	-0.0077114	0.15563	$K_{\mathrm{ms}1}$ $\left[\frac{\mathrm{N}}{\mathrm{mm}^2}\right]$	-0.2607102	-0.34898
Bl_2 $\left[\frac{\mathrm{N}}{\mathrm{Amm}^2}\right]$	-0.6019057	-0.1576	$K_{\mathrm{ms}2}$ $\left[\frac{\mathrm{N}}{\mathrm{mm}^3}\right]$	0.1466057	0.10891
Bl_3 $\left[\frac{\mathrm{N}}{\mathrm{Amm}^3}\right]$	-0.0016604	-0.0024596	$K_{\mathrm{ms}3}$ $\left[\frac{\mathrm{N}}{\mathrm{mm}^4}\right]$	-0.0049665	-0.0090764
Bl_4 $\left[\frac{\mathrm{N}}{\mathrm{Amm}^4}\right]$	0.0101072	0.0033673	$K_{\mathrm{ms}4}$ $\left[\frac{\mathrm{N}}{\mathrm{mm}^5}\right]$	0.0005919	0.0028738
$L_{\mathrm{e}0}$ [mH]	0.547	0.036			
$L_{\mathrm{e}1}$ $\left[\frac{\mathrm{mH}}{\mathrm{mm}}\right]$	-0.0478768	-0.016303			
$L_{\mathrm{e}2}$ $\left[\frac{\mathrm{mH}}{\mathrm{mm}^2}\right]$	-0.0113542	0.0018228			
$L_{\mathrm{e}3}$ $\left[\frac{\mathrm{mH}}{\mathrm{mm}^3}\right]$	0.0010058	0.00072416			
$L_{\mathrm{e}4}$ $\left[\frac{\mathrm{mH}}{\mathrm{mm}^4}\right]$	0.000113	-0.000060094			

4. Nonlinear Loudspeaker Model

According to [2], a nonlinear extension of the already presented linear model, capable of accurately describing the low-frequency behavior of loudspeakers even when excited with high-amplitude signals, is obtained by making some parameters (i.e., Bl, K_{ms}, and L_{e}) depend on the *displacement of the loudspeaker diaphragm* defined as

$$x(t) = \int I_{\mathrm{ms}}(t)\ \mathrm{d}t \tag{10}$$

where $I_{\mathrm{ms}}(t)$ is the diaphragm velocity as indicated in Fig. 1. The considered nonlinear loudspeaker model is hence characterized by the same circuit of the linear model in Fig. 1, but Bl, K_{ms}, and L_{e} are nonlinear and depend on $x(t)$.

4.1. Polynomial Models of Nonlinearities

To model the *nonlinear force factor* Bl as a function of $x(t)$ we choose a polynomial in the form

$$Bl\,(x(t)) = Bl_0 + Bl_1\,x(t) + Bl_2\,x^2(t) + Bl_3\,x^3(t) + Bl_4\,x^4(t)\ , \tag{11}$$

where the coefficients Bl_0, Bl_1, Bl_2, Bl_3, and Bl_4 are estimated from measured data according to the procedures described in [34, 44]. The gyrator connecting

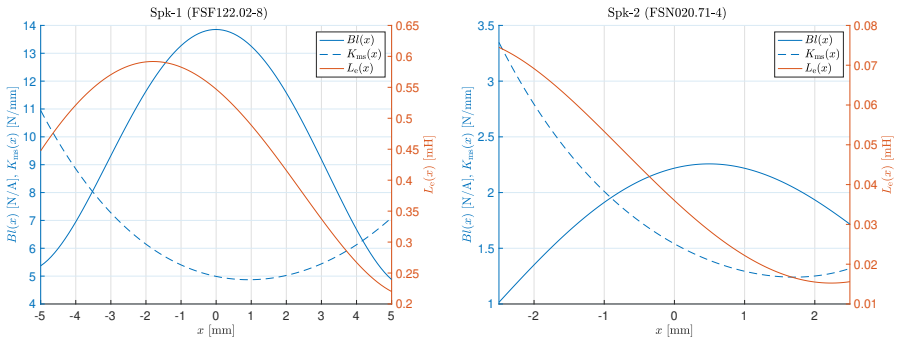

(a) (b)

Figure 5: Nonlinear curves of force factor Bl, nonlinear inductance L_{e}, and mechanical stiffness K_{ms}, all functions of the displacement x. (a) refers to Spk-1, while (b) refers to Spk-2.

the electrical part to the mechanical part is therefore characterized by the time-dependent gyration factor $Bl\,(x(t))$.

To model the *nonlinear inductive part of the voice coil impedance* L_{e} as a function of $x(t)$ we choose a polynomial in the form

$$L_{\mathrm{e}}\,(x(t)) = L_{\mathrm{e0}} + L_{\mathrm{e1}}\,x(t) + L_{\mathrm{e2}}\,x^2(t) + L_{\mathrm{e3}}\,x^3(t) + L_{\mathrm{e4}}\,x^4(t)\ , \qquad (12)$$

where the coefficients L_{e0}, L_{e1}, L_{e2}, L_{e3}, and L_{e4} are estimated from measured data [34, 44]. The inductor with inductance $L_{\mathrm{e}}(x(t))$ is therefore characterized by the equation

$$v(t) = \frac{\mathrm{d}\left[L_{\mathrm{e}}(x(t))i(t)\right]}{\mathrm{d}t} = L_{\mathrm{e}}(x(t))\frac{\mathrm{d}i(t)}{\mathrm{d}t} + i(t)\frac{\mathrm{d}L_{\mathrm{e}}(x(t))}{\mathrm{d}t}\ . \qquad (13)$$

To model the *nonlinear mechanical stiffness* K_{ms} as a function of $x(t)$ we choose a polynomial in the form

$$K_{\mathrm{ms}}\,(x(t)) = K_{\mathrm{ms0}} + K_{\mathrm{ms1}}\,x(t) + K_{\mathrm{ms2}}\,x^2(t) + K_{\mathrm{ms3}}\,x^3(t) + K_{\mathrm{ms4}}\,x^4(t)\ , \qquad (14)$$

where the coefficients K_{ms0}, K_{ms1}, K_{ms2}, K_{ms3}, and K_{ms4} are again estimated from measured data [34, 44]. The capacitor with capacitance $K_{\mathrm{ms}}^{-1}(x(t))$ is therefore characterized by the equation

$$i(t) = \frac{\mathrm{d}\left[K_{\mathrm{ms}}^{-1}(x(t))v(t)\right]}{\mathrm{d}t} = K_{\mathrm{ms}}^{-1}(x(t))\frac{\mathrm{d}v(t)}{\mathrm{d}t} + v(t)\frac{\mathrm{d}K_{\mathrm{ms}}^{-1}(x(t))}{\mathrm{d}t}\ . \qquad (15)$$

4.2. Estimation of Polynomial Coefficients

In this work, the coefficients of the polynomial nonlinearities of equations (11), (12), and (14) are estimated using the Klippel Analyzer System [34, 44]. The measured parameters of the three nonlinearities for loudspeakers Spk-1 and Spk-2 are reported in Table 4, while the corresponding curves are shown in the plots of Fig. 5.

5. Wave Digital Realization of the Nonlinear Loudspeaker Model

The proposed WD implementation of the nonlinear loudspeaker model is similar to the one of the linear model discussed in Section 3 and it does not require the use of iterative solvers. The implementation relies on the estimate of $x(t)$ and on the consequent update of $Bl(x(t))$, $L_{\mathrm{e}}(x(t))$ and $K_{\mathrm{ms}}(x(t))$ at each sampling step. This means that since some port resistances depend on the aforementioned three parameters they need to be updated at each sampling step; therefore, the scattering matrices of the WD junctions need to be updated as well.

In the discrete-time domain we compute the coil displacement using a unitary delay element such that we can implement the circuit in an explicit fashion. Therefore, at each sampling step we find an estimate $\widehat{x}[k]$ of the instantaneous coil displacement value as

$$\widehat{x}[k] = x[k-1] \ , \tag{16}$$

where

$$x[k-1] = \xi_x \left(T_{\mathrm{s}} \, I_{\mathrm{ms}}[k-1] + x[k-2] \right) \ . \tag{17}$$

ξ_x is a forgetting factor close to, but smaller than, one (e.g., $\xi_x = 0.9999$) whose role is to damp the local truncation error of numerical integration at each sampling step in such a way that it does not accumulate over simulation time. The velocity $I_{\mathrm{ms}}[k]$ is calculated as

$$I_{\mathrm{ms}}[k] = \frac{a_9[k] - b_9[k]}{2 Z_9[k]} \, . \tag{18}$$

5.1. Nonlinear Force Factor in the Discrete-Time Domain

At each sampling step, the nonlinear force factor is updated using the following expression

$$Bl(\widehat{x}[k]) = Bl_0 + Bl_1\,\widehat{x}[k] + Bl_2\,\widehat{x}^2[k] + Bl_3\,\widehat{x}^3[k] + Bl_4\,\widehat{x}^4[k] \ . \tag{19}$$

5.2. Nonlinear Voice Coil Inductive Impedance in the Discrete-Time Domain

In order to derive the discrete-time implementation of the nonlinear inductor, let us rewrite the continuous-time constitutive equation (13) as

$$v(t) = L_{\rm e}(x(t))\frac{{\rm d}i(t)}{{\rm d}t} + i(t)L'_{\rm e}(x(t))\frac{{\rm d}x(t)}{{\rm d}t} \ , \tag{20}$$

where

$$L'_{\rm e}(x(t)) = \frac{{\rm d}L_{\rm e}(x(t))}{{\rm d}x} = L_{\rm e1} + 2\,L_{\rm e2}\,x(t) + 3\,L_{\rm e3}\,x^2(t) + 4\,L_{\rm e4}\,x^3(t) \ , \tag{21}$$

and

$$\frac{{\rm d}x(t)}{{\rm d}t} = I_{\rm ms}(t) \ . \tag{22}$$

Let us approximate equation (20) in the discrete-time domain as

$$v[k] = L_{\rm e}[k]\frac{i[k] - \xi_{L_{\rm e}} i[k-1]}{T_{\rm s}} + i[k]L'_{\rm e}[k]\widehat{I}_{\rm ms}[k]\,, \tag{23}$$

where

$$\widehat{I}_{\rm ms}[k] = I_{\rm ms}[k-1] \ , \tag{24}$$

$$L_{\rm e}[k] = L_{\rm e}(\widehat{x}[k]) = L_{\rm e0} + L_{\rm e1}\,\widehat{x}[k] + L_{\rm e2}\,\widehat{x}^2[k] + L_{\rm e3}\,\widehat{x}^3[k] + L_{\rm e4}\,\widehat{x}^4[k]\,, \tag{25}$$

$$L'_{\rm e}[k] = L'_{\rm e}(\widehat{x}[k]) = \frac{{\rm d}L_{\rm e}(\widehat{x}[k])}{{\rm d}x} = L_{\rm e1} + 2\,L_{\rm e2}\,\widehat{x}[k] + 3\,L_{\rm e3}\,\widehat{x}^2[k] + 4\,L_{\rm e4}\,\widehat{x}^3[k], \tag{26}$$

and $\xi_{L_{\rm e}}$ is a forgetting factor close to, but smaller than, one (e.g., $\xi_{L_{\rm e}} = 0.9999$) whose role is to damp the local truncation error of numerical differentiation. Rearranging equation (23) we get

$$v[k] = \left(L'_{\rm e}[k]\widehat{I}_{\rm ms}[k] + \frac{L_{\rm e}[k]}{T_{\rm s}}\right) i[k] - \xi_{L_{\rm e}} i[k-1]\frac{L_{\rm e}[k]}{T_{\rm s}}\,. \tag{27}$$

The discrete-time Kirchhoff constitutive equation (27) of the time-variant inductor can be expressed in the WD domain as

$$b[k] = \xi_{L_\mathrm{e}} \left(b[k-1] - a[k-1] \right) \frac{L_\mathrm{e}[k]}{2T_\mathrm{s} Z[k-1]} \,, \tag{28}$$

$$\text{with } \; Z[k] = L'_\mathrm{e}[k] \widehat{I}_\mathrm{ms}[k] + \frac{L_\mathrm{e}[k]}{T_\mathrm{s}} \,. \tag{29}$$

5.3. Nonlinear Mechanical Stiffness in the Discrete-Time Domain

Equation (15) can be rewritten as

$$i(t) = \frac{1}{K_\mathrm{ms}\left(x(t)\right)} \frac{\mathrm{d}v(t)}{\mathrm{d}t} + v(t) C'_\mathrm{ms}(x(t)) \frac{\mathrm{d}x(t)}{\mathrm{d}t} \;\; , \tag{30}$$

or equivalently

$$i(t) = \frac{1}{K_\mathrm{ms}\left(x(t)\right)} \frac{\mathrm{d}v(t)}{\mathrm{d}t} + v(t) i(t) C'_\mathrm{ms}(x(t)) \;\; , \tag{31}$$

since $\frac{\mathrm{d}x(t)}{\mathrm{d}t} = I_\mathrm{ms}(t) = i(t)$, where

$$C'_\mathrm{ms}(x(t)) = -\frac{K'_\mathrm{ms}\left(x(t)\right)}{K^2_\mathrm{ms}(x(t))} = \frac{K_\mathrm{ms1} + 2\,K_\mathrm{ms2}\,x(t) + 3\,K_\mathrm{ms3}\,x^2(t) + 4\,K_\mathrm{ms4}\,x^3(t)}{-K^2_\mathrm{ms}(x(t))} \,. \tag{32}$$

We approximate equation (31) in the discrete-time domain as

$$i[k] = \frac{v[k] - \xi_{C_\mathrm{ms}} v[k-1]}{T_\mathrm{s} K_\mathrm{ms}[k]} + i[k] v[k-1] C'_\mathrm{ms}[k] \;\; , \tag{33}$$

where

$$K_\mathrm{ms}[k] = K_\mathrm{ms}(\widehat{x}[k]) = K_\mathrm{ms0} + K_\mathrm{ms1}\,\widehat{x}[k] + K_\mathrm{ms2}\,\widehat{x}^2[k] + K_\mathrm{ms3}\,\widehat{x}^3[k] + K_\mathrm{ms4}\,\widehat{x}^4[k] \,, \tag{34}$$

$$C'_\mathrm{ms}[k] = C'_\mathrm{ms}(\widehat{x}[k]) = -\frac{K'_\mathrm{ms}\left(\widehat{x}[k]\right)}{K^2_\mathrm{ms}(\widehat{x}[k])} \;\; , \tag{35}$$

$$K'_\mathrm{ms}\left(\widehat{x}[k]\right) = K_\mathrm{ms1} + 2\,K_\mathrm{ms2}\,\widehat{x}[k] + 3\,K_\mathrm{ms3}\,\widehat{x}^2[k] + 4\,K_\mathrm{ms4}\,\widehat{x}^3[k] \;\; , \tag{36}$$

and ξ_{C_ms} is a forgetting factor close to, but smaller than, one (e.g., $\xi_{C_\mathrm{ms}} = 0.9999$).

Rearranging equation (33) we get

$$v[k] = K_\mathrm{ms}[k]\, T_\mathrm{s} \left(1 - v[k-1] C'_\mathrm{ms}[k]\right) i[k] + \xi_{C_\mathrm{ms}}\, v[k-1] \;\; . \tag{37}$$

The discrete-time Kirchhoff constitutive equation (37) of the time-variant capacitor can be expressed in the WD domain as

$$b[k] = \xi_{C_{\mathrm{ms}}} \frac{a[k-1] + b[k-1]}{2} \ , \tag{38}$$

$$\text{with} \quad Z[k] = K_{\mathrm{ms}}[k]\, T_{\mathrm{s}} \left(1 - C'_{\mathrm{ms}}[k] \frac{a[k-1] + b[k-1]}{2}\right) . \tag{39}$$

5.4. Nonlinear WDF Model Validation

In this subsection, we validate the behavior of the nonlinear WDF model; firstly, by comparing the results of its MATLAB implementation with SPICE simulations, again performed with the Electrical Circuit interface of COMSOL Multiphysics; and then with signals measured from the two already described loudspeaker systems, Spk-1 and Spk-2, driven by mid- and high-amplitude signals. In particular, the generic driving voltage signal is defined as

$$V_{\mathrm{in}}(t) = A_{\mathrm{in}} \frac{s_{\mathrm{in}}(t)}{\mathrm{rms}\{s_{\mathrm{in}}(t)\}} \tag{40}$$

where A_{in} is an amplitude parameter in $\mathrm{V_{rms}}$, rms{.} is an operator returning the root mean square value of the argument, while $s_{\mathrm{in}}(t)$ is the dimensionless input signal. We perform three sets of experiments characterized by three different kinds of signals $s_{\mathrm{in}}(t)$: sinusoids, 2-tone signals, and a music signal. Comparisons between WDF results, SPICE results, and measured data are provided both in the time domain and in the frequency domain. The employed measurement setup is the same used for validating the linear WDF model and it is described in Appendix A. The coefficients of the polynomial nonlinearities of the two loudspeakers are reported in Table 4, while the parameters of linear elements are those in Table 2. The sampling frequency set in the WDF simulations is $F_{\mathrm{s}} = 96$ kHz.

In the first set of experiments, the dimensionless input signals are sinusoids in the form $s_{\mathrm{in}}(t) = \sin(2\pi f_{\mathrm{in}} t)$, where f_{in} is the fundamental frequency in Hz. Defined for each loudspeaker the resonance frequency, i.e., the frequency corresponding to the maximum value of function $|\mathcal{Z}_{\mathrm{e}}|$ in Fig. 4, as f_{r}, we perform experiments in which we set $f_{\mathrm{in}} = f_{\mathrm{r}}/2$ and $f_{\mathrm{in}} = 2f_{\mathrm{r}}$ and we vary A_{in}.

In the second set of experiments, the dimensionless input signals are 2-tones expressed as $s_{\text{in}}(t) = \sin(2\pi f_{\text{in1}} t + \varphi_{\text{in1}}) + \sin(2\pi f_{\text{in2}} t + \varphi_{\text{in2}})$, where f_{in1} and f_{in2} are the fundamental frequencies of the two sinusoids, while φ_{in1} and φ_{in2} are random phase parameters. The amplitude parameter A_{in} is varied in the different experiments.

In the third set of experiments, $s_{\text{in}}(t)$ is a music signal, i.e., the first 10 seconds of the recording "*So tired*" by E. Clapton, obtained as the average between the 2 stereo channels in order to get a mono signal. Also in this case, the amplitude parameter A_{in} is varied in the different experiments.

Fig. 6, Fig. 7, and Fig. 8 are referred to the first, the second, and the third set of aforementioned experiments, respectively. They show comparisons between real measures of the output pressure signal P_{out}, results of WDF simulations, and results of SPICE simulations, both in the time domain and in the frequency domain through the evaluation of the Power Spectral Density (PSD). The values of input signal parameters used in each experiment are written on every corresponding plot. Table 5 reports both the Normalized Root Mean Square Error (NRMSE) between the measured P_{out} signal and corresponding WDF simulation output and the NRMSE between the measured P_{out} signal and the SPICE simulation output for each experiment related to Spk-1. Table 6 does the same for experiments related to Spk-2.

Looking at Fig. 6, Fig. 7, and Fig. 8, we can see that, in all the experiments, the matching between proposed WDF results and SPICE results is near-perfect, as the corresponding curves are generally superimposed. Also the matching between measured signals and outputs of digital simulations is almost perfect and it confirms the ability of the circuital model to capture the loudspeaker behavior even dealing with high-amplitude input signals. It is interesting to notice that the ranges of NRMSE values in Table 5 and in Table 6 are in the same order of magnitude for all the experiments, suggesting that the considered circuital model of loudspeakers is characterized by similar accuracy performance when different input signals are considered. Moreover, the values in the two columns named "NRMSE WDF" and "NRMSE SPICE" are really close, again

Table 5: Spk-1 (FSF122.02-8) - NRMSE of Digital Models for Different $V_{\text{in}}(t)$ Signals

	$V_{\text{in}}(t)$ **Signal Parameters**	**NRMSE WDF**	**NRMSE SPICE**
Sinusoids	$A_{\text{in}} = 4$ V_{rms}, $f_{\text{in}} = 28.75$ Hz	0.014356	0.035917
	$A_{\text{in}} = 11.5$ V_{rms}, $f_{\text{in}} = 28.75$ Hz	0.017774	0.035538
	$A_{\text{in}} = 4$ V_{rms}, $f_{\text{in}} = 115$ Hz	0.010293	0.026658
	$A_{\text{in}} = 11.5$ V_{rms}, $f_{\text{in}} = 115$ Hz	0.012417	0.02601
2-Tones	$A_{\text{in}} = 4$ V_{rms}, $f_{\text{in1}} = 28.75$ Hz, $f_{\text{in2}} = 121.78$ Hz	0.012172	0.034109
	$A_{\text{in}} = 7.5$ V_{rms}, $f_{\text{in1}} = 28.75$ Hz, $f_{\text{in2}} = 121.78$ Hz	0.014454	0.038661
	$A_{\text{in}} = 11.5$ V_{rms}, $f_{\text{in1}} = 28.75$ Hz, $f_{\text{in2}} = 121.78$ Hz	0.015543	0.040685
Music Sig.	$A_{\text{in}} = 4$ V_{rms}	0.0103	0.036996
	$A_{\text{in}} = 7.5$ V_{rms}	0.014615	0.046251
	$A_{\text{in}} = 11.5$ V_{rms}	0.017743	0.054391

confirming that the proposed explicit WDF implementation has the same level of accuracy of the SPICE implementation.

As far as the efficiency performance of the proposed WDF model is concerned, its MATLAB implementation runs with an average execution time of approximately 0.3 μs per sample, which is lower than $T_{\text{s}} = 1/F_{\text{s}} = 1/(96\text{ kHz}) = 10.417\ \mu s$. This means that the MATLAB implementation of the proposed WDF can be executed on the fly.

6. Conclusions

In this manuscript we presented a WDF realization of a nonlinear lumped model of dynamic loudspeaker composed of three interdependent subcircuits representing the electrical part, the mechanical part, and the acoustical part of the transducer system. The proposed discrete-time implementation of the model is highly modular, as each one-port circuit element is represented as an input-output block by exploiting WDF principles. The accuracy of the presented nonlinear WDF has been verified by comparing its behavior with SPICE simulations of the reference circuit and with data measured from two real loud-

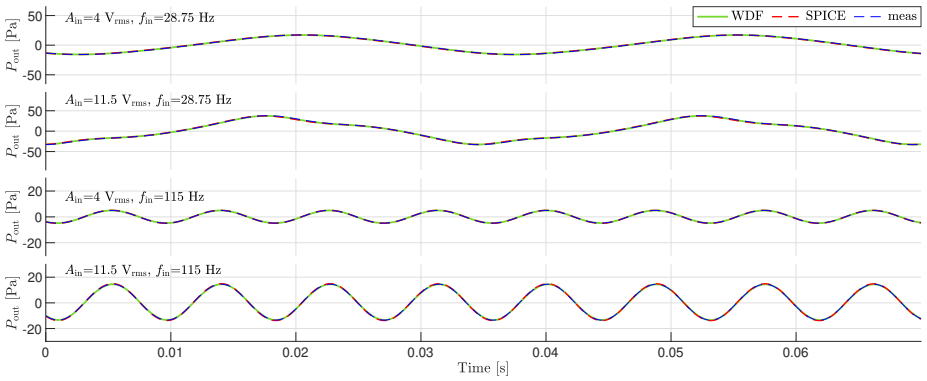

(a) Spk-1 (FSF122.02-8)

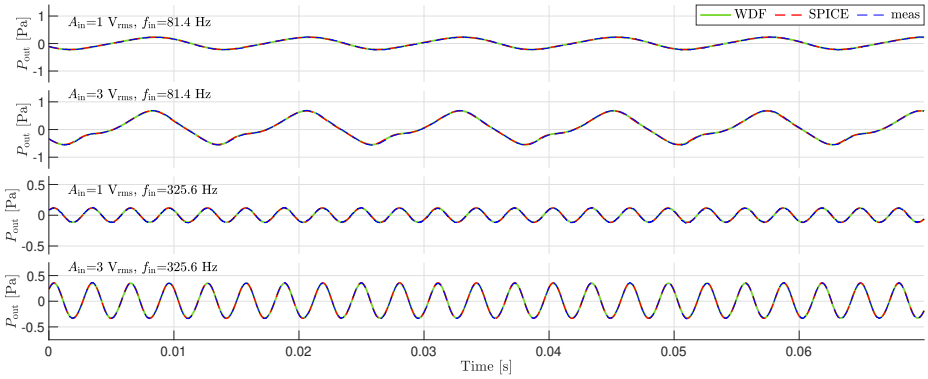

(b) Spk-2 (FSN020.71-4)

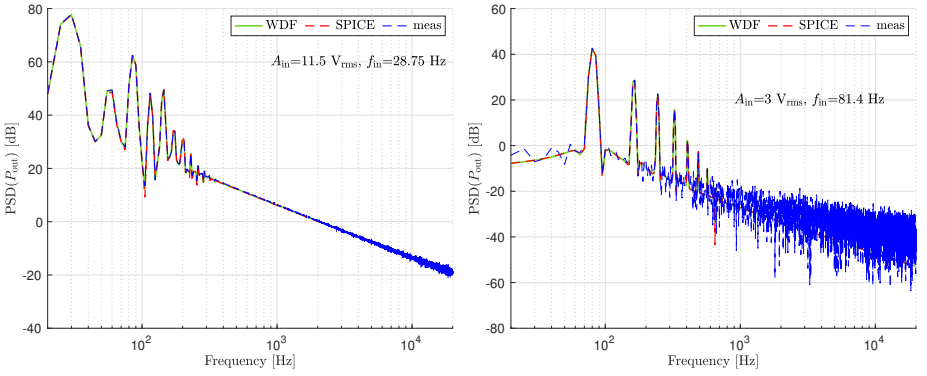

(c) Spk-1 (FSF122.02-8)

(d) Spk-2 (FSN020.71-4)

Figure 6: Nonlinear WDF model validation. Experiments with sinusoidal input signals. Comparisons between WDF results, SPICE results, and measured signals from Spk-1 and Spk-2 with different configurations of input signal parameters. (a) and (b) show P_{out} signals in the time domain. (c) and (d) show the PSD of P_{out} signals in the frequency domain.

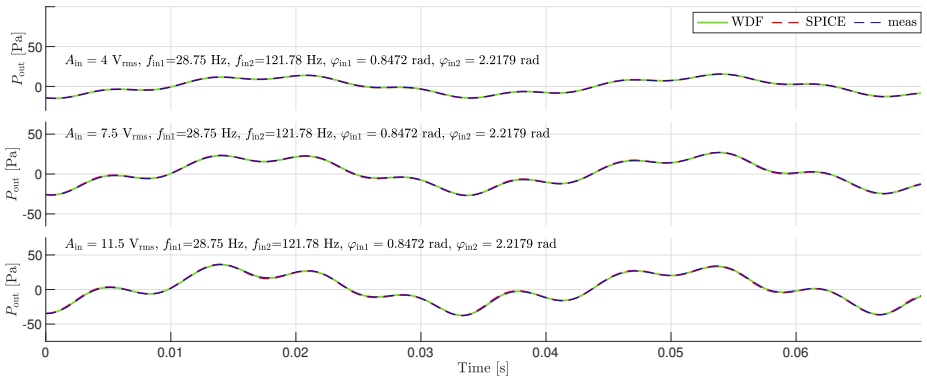

(a) Spk-1 (FSF122.02-8)

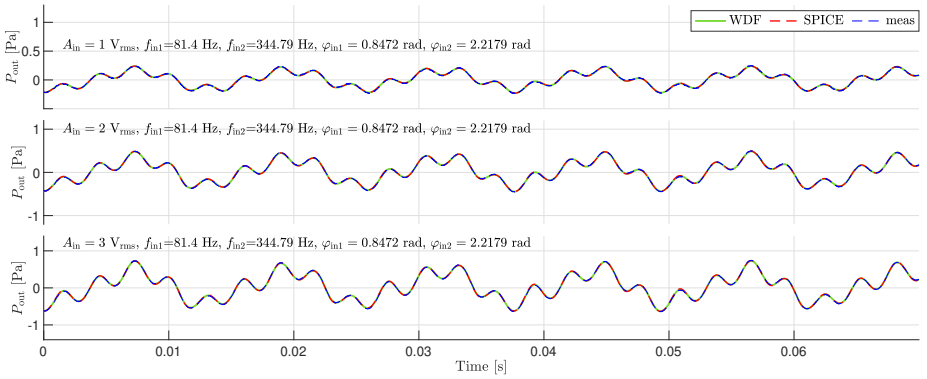

(b) Spk-2 (FSN020.71-4)

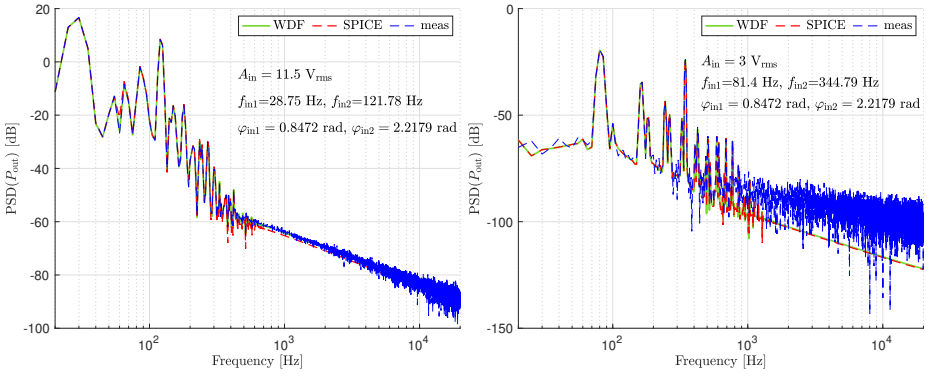

(c) Spk-1 (FSF122.02-8)

(d) Spk-2 (FSN020.71-4)

Figure 7: Nonlinear WDF model validation. Experiments with 2-tone input signals. Comparisons between WDF results, SPICE results, and measured signals from Spk-1 and Spk-2 with different configurations of input signal parameters. (a) and (b) show P_{out} signals in the time domain. (c) and (d) show the PSD of P_{out} signals in the frequency domain.

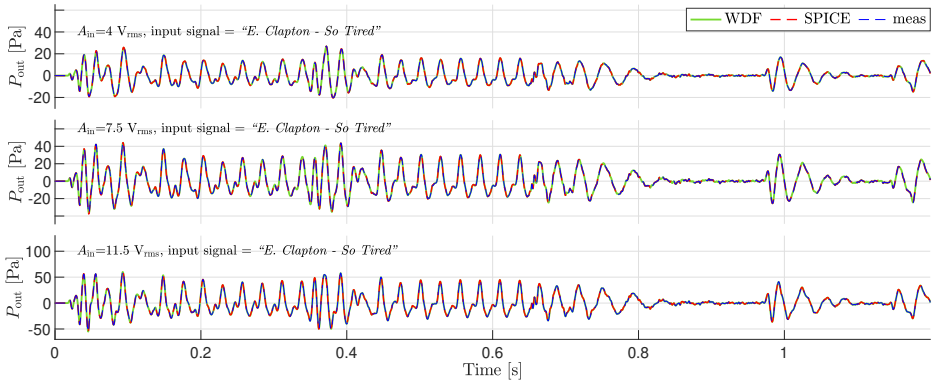

(a) Spk-1 (FSF122.02-8)

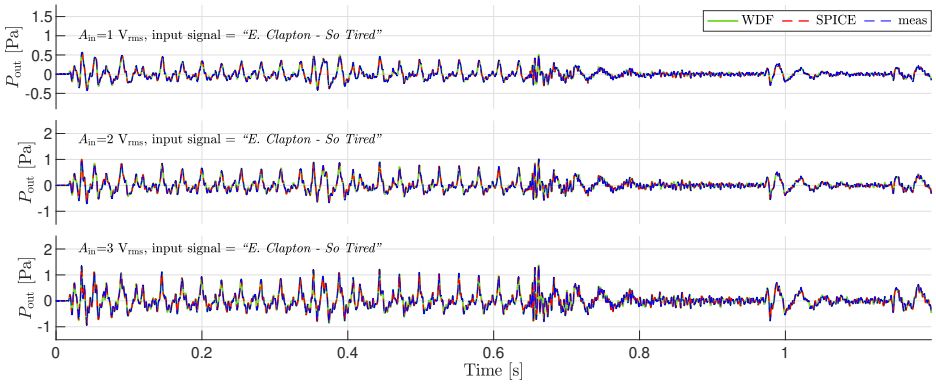

(b) Spk-2 (FSN020.71-4)

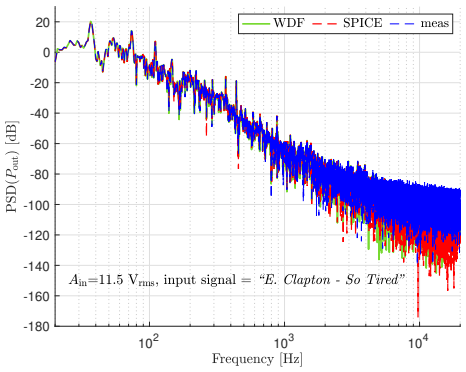

(c) Spk-1 (FSF122.02-8)

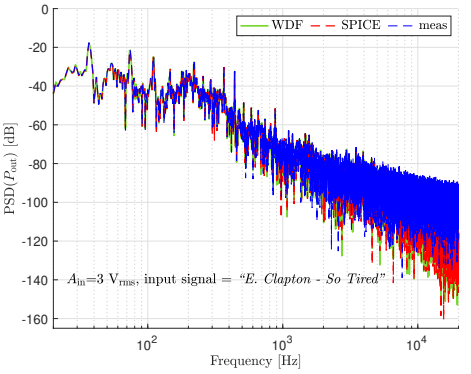

(d) Spk-2 (FSN020.71-4)

Figure 8: Nonlinear WDF model validation. Experiments with musical input signals. Comparisons between WDF results, SPICE results, and measured signals from Spk-1 and Spk-2 with different configurations of input signal parameters. (a) and (b) show P_{out} signals in the time domain. (c) and (d) show the PSD of P_{out} signals in the frequency domain.

Table 6: Spk-2 (FSN020.71-4) - NRMSE of Digital Models for Different $V_{\text{in}}(t)$ Signals

	$V_{\text{in}}(t)$ **Signal Parameters**	**NRMSE WDF**	**NRMSE SPICE**
Sinusoids	$A_{\text{in}} = 1$ V_{rms}, $f_{\text{in}} = 81.4$ Hz	0.039413	0.047134
	$A_{\text{in}} = 3$ V_{rms}, $f_{\text{in}} = 81.4$ Hz	0.021734	0.036001
	$A_{\text{in}} = 1$ V_{rms}, $f_{\text{in}} = 325.6$ Hz	0.066697	0.067224
	$A_{\text{in}} = 3$ V_{rms}, $f_{\text{in}} = 325.6$ Hz	0.026501	0.025626
2-Tones	$A_{\text{in}} = 1$ V_{rms}, $f_{\text{in1}} = 81.4$ Hz, $f_{\text{in2}} = 344.79$ Hz	0.047501	0.053242
	$A_{\text{in}} = 2$ V_{rms}, $f_{\text{in1}} = 81.4$ Hz, $f_{\text{in2}} = 344.79$ Hz	0.028176	0.037087
	$A_{\text{in}} = 3$ V_{rms}, $f_{\text{in1}} = 81.4$ Hz, $f_{\text{in2}} = 344.79$ Hz	0.022492	0.034156
Music Sig.	$A_{\text{in}} = 1$ V_{rms}	0.045245	0.051218
	$A_{\text{in}} = 2$ V_{rms}	0.028884	0.038923
	$A_{\text{in}} = 3$ V_{rms}	0.024178	0.038673

speakers of different sizes. The proposed WDF is fully explicit, as it does not need any iterative solver for computing the circuit signals; and it is highly efficient, as confirmed by the fact that its MATLAB implementation is able to process the input signal on the fly. It follows that the proposed WDF can be integrated in digital signal processing algorithms for linearization, equalization, or, more generally, virtualization of loudspeakers. This will be demonstrated in the second part of this two-part work [43].

Appendix A. Measurement Setup

The scheme in Fig. A.9 shows the structure of the measurement setup. A custom-made MATLAB-based measurement software generates the audio signals, feeding the D/A converter in the audio interface RME Fireface UFX II. The analog signal from the D/A converter is amplified by a Crown MA-5002VZ audio amplifier whose output feeds the loudspeaker under test. The rear surface of the loudspeaker is loaded by a closed box in which a Earthworks M30 microphone is installed to sense the pressure generated by the loudspeaker in the box. The front face of the loudspeaker radiates in a low-reverberation chamber

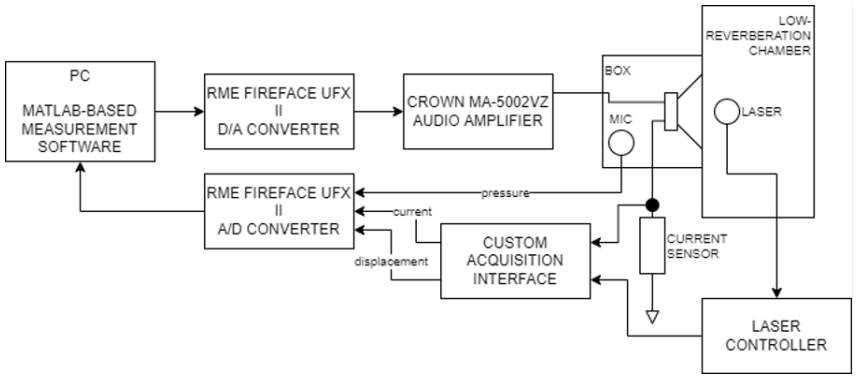

Figure A.9: Scheme of the measurement setup.

to minimize the effect of front loading. The displacement of the loudspeaker diaphragm is sensed by a Panasonic ANR1282 laser with ANR5132 controller. The current through the loudspeaker voice coil is sensed using a 0.03 ohm shunt resistor. Laser and current signals are conditioned by a custom acquisition interface to protect the inputs of the interface RME Fireface UFX II A/D converters, while the microphone signal goes directly to the interface input. The acquired signals are recorded and processed by the MATLAB-based measurement software.

Acknowledgements

The research work presented in this article was founded by Elettromedia s.p.a., Strada Regina km 3.500, 62018 Potenza Picena (MC), Italy.

References

[1] P. M. Brunet, Nonlinear system modeling and identification of loudspeakers, Ph.D. Dissertation, Northeastern University, Boston, Mass. (USA) (April 2014).

[2] W. Klippel, Tutorial: Loudspeaker nonlinearities—causes, parameters, symptoms, J. Audio Eng. Soc 54 (10) (2006) 907–939.
URL `http://www.aes.org/e-lib/browse.cfm?elib=13881`

[3] W. A. Frank, An efficient approximation to the quadratic volterra filter and its application in real-time loudspeaker linearization, Signal Processing 45 (1) (1995) 97 – 113. doi:https://doi.org/10.1016/0165-1684(95)00044-E.

[4] H. Schurer, C. H. Slump, O. E. Herrmann, Exact input-output linearization of an electrodynamical loudspeaker, in: Proc. 101st Audio Engineering Society Convention (AES), 1996.
URL http://www.aes.org/e-lib/browse.cfm?elib=7445

[5] D. Franken, K. Meerkotter, J. Wassmuth, Observer-based feedback linearization of dynamic loudspeakers with ac amplifiers, IEEE Transactions on Speech and Audio Processing 13 (2) (2005) 233–242. doi:10.1109/TSA.2004.841043.

[6] S. S. Payal, V. J. Mathews, A. Iyer, R. Lambert, J. Hutchings, Equalization of excursion and current-dependent nonlinearities in loudspeakers, in: 2014 IEEE International Conference on Acoustics, Speech and Signal Processing (ICASSP), 2014, pp. 6697–6701. doi:10.1109/ICASSP.2014.6854896.

[7] B. Defraene, T. van Waterschoot, M. Diehl, M. Moonen, Embedded-optimization-based loudspeaker precompensation using a hammerstein loudspeaker model, IEEE/ACM Transactions on Audio, Speech, and Language Processing 22 (11) (2014) 1648–1659. doi:10.1109/TASLP.2014.2344862.

[8] A. Falaize, N. Papazoglou, T. Helie, N. Lopes, Compensation of loudspeaker's nonlinearities based on flatness and port-hamiltonian ap-proach, in: Proc. 22eme Congres Francais de Mechanique, 2015.

[9] H. Nakajima, N. Sakata, K. Hashino, Non-linear distortion reduction for a loudspeaker based on recursive source equalization, in: Proc. IEEE Int. Conf. on Acoustics, Speech and Signal Process., 2015.

[10] Y. Kadowaki, T. Samejima, Nonlinear distortion reduction of an electrodynamic loudspeaker by using model-following control theory, Acoust. Sci. & Tech. 38 (4) (2017) 1–3.

[11] H. Merabti, D. Massicotte, W. P. Zhu, Electrodynamic loudspeaker linearization using a low complexity pth-order inverse non-linear filter, in: Proc. IEEE Int. Symp. on Signal Processing and Information Technology, 2019.

[12] E. Yudaningtyas, A. Khabib, W. Djuriatno, D. J. D. H. Santjojo, A. Muttaquin, P. Siwindarto, Z. Amalia, Nonlinearity compensation of low-frequency loudspeaker response using internal model controller, Telekomnika 17 (2) (2019) 946–955.

[13] X. Tian, W. Liu, X. Feng, Y. Shen, Compensation of nonlinear distortion in loudspeakers considering nonlinear viscoelasticity of the suspension, J. Audio Eng. Soc. 69 (3) (2021) 204–210.

[14] Lu, Tianjian, Smedegaard, Michael, Wu, Ken, Multiphysics modeling of voice coil actuators with recurrent neural network, IEEE Journal on Multiscale and Multiphysics Computational Techniques 4 (2019) 12–19. doi:10.1109/JMMCT.2019.2891672.

[15] H.-K. Jang, K.-J. Kim, Identification of loudspeaker nonlinearities using the narmax modeling technique, Journal of the audio engineering society 42 (1/2) (1994) 50–59.
URL http://www.aes.org/e-lib/browse.cfm?elib=6961

[16] A. J. M. Kaizer, Modeling of the Nonlinear Response of an Electrodynamic Loudspeaker by a Volterra Series Expansion, J. Audio Eng. Soc. 35 (6) (1987) 421–433.

[17] K. Lashkari, A Modified Volterra-Wiener-Hammerstein Model for Loudspeaker Precompensation, in: Conference Record of the Thirty-Ninth Asilo-

mar Conference on Signals, Systems and Computers, 2005., 2005, pp. 344–348. doi:10.1109/ACSSC.2005.1599765.

[18] N. Thiele, Loudspeakers in vented boxes: Part 1, Journal of the Audio Engineering Society 19 (5) (1971) 382–392.
URL http://www.aes.org/e-lib/browse.cfm?elib=2173

[19] R. H. Small, Closed-box loudspeaker systems–part 1: Analysis, Journal of the Audio Engineering Society 20 (10) (1972) 798–808.
URL http://www.aes.org/e-lib/browse.cfm?elib=2022

[20] R. H. Small, Vented-box loudspeaker systems–part 1: Small-signal analysis, Journal of the Audio Engineering Society 21 (5) (1973) 363–372.
URL http://www.aes.org/e-lib/browse.cfm?elib=1967

[21] U. Seidel, W. Klippel, Fast and accurate measurement of the linear transducer parameters, in: Audio Engineering Society Convention 110, 2001.
URL http://www.aes.org/e-lib/browse.cfm?elib=9988

[22] D. Franken, K. Meerkotter, J. Wassmuth, Passive parametric modeling of dynamic loudspeakers, IEEE Transactions on Speech and Audio Processing 9 (8) (2001) 885–891. doi:10.1109/89.966091.

[23] M. Kleiner, Electroacoustics, Taylor & Francis Group, LLC, Boca Raton, FL, USA, 2013.

[24] L. Beranek, T. Mellow, Acoustics. Sound Fields, Transducers and Vibration, 2nd Edition, Academic Press, London, UK, 2019.

[25] A. Falaize, T. Hélie, Passive modelling of the electrodynamic loudspeaker: from the Thiele-Small model to nonlinear port-Hamiltonian systems, Acta Acust. 4 (1) (2020) 1. doi:10.1051/aacus/2019001.
URL https://doi.org/10.1051/aacus/2019001

[26] R. H. Small, Direct-radiator loudspeaker system analysis, IEEE Transactions on Audio and Electroacoustics AU-19 (4) (1971) 269–281.

[27] A. Falaize, T. Hélie, Passive guaranteed simulation of analog audio circuits: A port-hamiltonian approach, Appl. Sci. 6 (10).

[28] G. Moretti, G. Rizzello, M. Fontana, S. Seelecke, A multi-domain dynamical model for cone-shaped dielectric elastomer loudspeakers, in: I. A. Anderson, H. R. Shea, J. D. W. Madden (Eds.), Proc. SPIE 11587, Electroactive Polymer Actuators and Devices (EAPAD) XXIII, International Society for Optics and Photonics, 2021, pp. 226 – 239. doi:10.1117/12.2581718.

[29] J. Huang, X. Feng, S. Chen, Y. Shen, Analysis of total harmonic distortion of miniature loudspeakers used in mobile phones considering nonlinear acoustic damping, The Journal of the Acoustical Society of America 149 (3) (2021) 1579–1588. arXiv:https://doi.org/10.1121/10.0003644, doi:10.1121/10.0003644.

[30] R. Liechti, S. Durand, T. Hilt, F. Casset, C. Poulain, G. Le Rhun, F. Pavageau, H. Kuentz, M. Colin, Total Harmonic Distortion of a Piezoelectric MEMS Loudspeaker in an IEC 60318-4 Coupler Estimation Using Static Measurements and a Nonlinear State Space Model, Micromachines 12 (12). doi:10.3390/mi12121437.

[31] J. Schmith, L. P. Luna de Oliveira, Dimensioning sealed enclosures for suppressing nonlinear distortions in woofers, Applied Acoustics 178 (2021) 107975. doi:https://doi.org/10.1016/j.apacoust.2021.107975.

[32] W. Klippel, Modeling and testing of loudspeakers used in sound-field control, in: D. B. F. Katz, D. P. Majdak (Eds.), Advances in Fundamental and Applied Research on Spatial Audio, IntechOpen, Rijeka, 2022, Ch. 5. doi:10.5772/intechopen.102029.

[33] J. F. Lazar, P. M. Brunet, Reluctance force compensation for the nonlinear control of a loudspeaker, in: Proc. 149th AES Conv., 2020.

[34] W. Klippel, Distortion analyzer-a new tool for assessing and improving electrodynamic transducer, in: Audio Engineering Society Convention 108,

2000.
URL http://www.aes.org/e-lib/browse.cfm?elib=9229

[35] W. Klippel, Measurement of large-signal parameters of electrodynamic transducer, in: Proc. 107th AES Conv., 1999.

[36] A. Fettweis, Wave digital filters: Theory and practice, Proc. IEEE 74 (2) (1986) 270–327.

[37] K. Meerkötter, R. Scholz, Digital simulation of nonlinear circuits by wave digital filter principles, in: IEEE Int. Symp. Circuits Syst., 1989, pp. 720–723.

[38] S. Bilbao, Wave and Scattering Methods for Numerical Simulation, 1st Edition, Chichester, UK, 2004.

[39] A. Bernardini, P. Maffezzoni, L. Daniel, A. Sarti, Wave-based analysis of large nonlinear photovoltaic arrays, IEEE Transactions on Circuits and Systems I: Regular Papers 65 (4) (2018) 1363–1376. doi:10.1109/TCSI.2017.2756917.

[40] K. J. Werner, A. Bernardini, J. O. Smith, A. Sarti, Modeling circuits with arbitrary topologies and active linear multiports using wave digital filters, IEEE Transactions on Circuits and Systems I: Regular Papers 65 (12) (2018) 4233–4246. doi:10.1109/TCSI.2018.2837912.

[41] A. Bernardini, E. Bozzo, F. Fontana, A. Sarti, A wave digital newton-raphson method for virtual analog modeling of audio circuits with multiple one-port nonlinearities, IEEE/ACM Transactions on Audio, Speech, and Language Processing 29 (2021) 2162–2173. doi:10.1109/TASLP.2021.3084337.

[42] A. Bernardini, P. Maffezzoni, A. Sarti, Linear multistep discretization methods with variable step-size in nonlinear wave digital structures for virtual analog modeling, IEEE/ACM Transactions on Audio, Speech, and

Language Processing 27 (11) (2019) 1763–1776. doi:10.1109/TASLP.2019.2931759.

[43] A. Bernardini, L. Bianchi, A. Sarti, Loudspeaker Virtualization–Part II: The Inverse Transducer Model and the Direct-Inverse-Direct Chain, accepted for publication in Signal Processing.

[44] Klippel GmbH, Klippel Analyzer Official Website.
URL https://www.klippel.de/products/rd-system/analyzer-hardware/ka3-klippel-analyzer-3.html

[45] G. O. Martens, K. Meerkötter, On N-port adaptors for wave digital filters with application to a bridged-tee filter, in: Proc. IEEE Int. Symp. Circuits Syst. (ISCAS), Munich, Germany, 1976, pp. 514–517.

[46] A. Bernardini, K. J. Werner, J. O. Smith, A. Sarti, Generalized wave digital filter realizations of arbitrary reciprocal connection networks, IEEE Trans. Circuits and Systems I: Regular Papers 66 (2) (2019) 694–707. doi:10.1109/TCSI.2018.2867508.

[47] R. Giampiccolo, M. G. De Bari, A. Bernardini, A. Sarti, Wave digital modeling and implementation of nonlinear audio circuits with nullors, IEEE/ACM Transactions on Audio, Speech, and Language Processing (2021) 1–1doi:10.1109/TASLP.2021.3120627.

[48] A. Sarti, G. De Sanctis, Systematic methods for the implementation of nonlinear wave-digital structures, IEEE Trans. Circuits Syst. I, Reg. Papers 56 (2009) 460–472.